0026-895X/05/6706-1874–1881$20.00
MOLECULAR PHARMACOLOGY
Copyright © 2005 The American Society for Pharmacology and Experimental Therapeutics
Mol Pharmacol 67:1874–1881, 2005

Vol. 67, No. 6
9944/3034724
Printed in U.S.A.

The Crystal Structure of the Complex of the Anticancer Prodrug 7-Ethyl-10-[4-(1-piperidino)-1-piperidino]-carbonyloxycamptothecin (CPT-11) with *Torpedo californica* Acetylcholinesterase Provides a Molecular Explanation for Its Cholinergic Action

Michal Harel, Janice L. Hyatt, Boris Brumshtein, Christopher L. Morton, Kyoung Jin P. Yoon, Randy M. Wadkins, Israel Silman, Joel L. Sussman, and Philip M. Potter

Department of Structural Biology, Weizmann Institute of Science, Rehovot, Israel (M.H., B.B., J.L.S.); Department of Molecular Pharmacology, St. Jude Children's Research Hospital, Memphis, Tennessee (J.L.H., C.L.M., K.J.P.Y., P.M.P.); Department of Chemistry and Biochemistry, University of Mississippi, University, Mississippi (R.M.W.); and Department of Neurobiology, Weizmann Institute of Science, Rehovot, Israel (I.S.)

Received December 2, 2004; accepted March 16, 2005

ABSTRACT

The anticancer prodrug 7-ethyl-10-[4-(1-piperidino)-1-piperidino-]carbonyloxycamptothecin (CPT-11) is a highly effective camptothecin analog that has been approved for the treatment of colon cancer. It is hydrolyzed by carboxylesterases to yield 7-ethyl-10-hydroxycamptothecin (SN-38), a potent topoisomerase I poison. However, upon high-dose intravenous administration of CPT-11, a cholinergic syndrome is observed that can be ameliorated by atropine. Previous studies have indicated that CPT-11 can inhibit acetylcholinesterase (AChE), and here, we provide a detailed analysis of the inhibition of AChE by CPT-11 and by structural analogs. These studies demonstrate that the terminal dipiperidino moiety in CPT-11 plays a major role in enzyme inhibition, and this has been confirmed by X-ray crystallographic studies of a complex of the drug with *Torpedo californica* AChE. Our results indicate that CPT-11 binds within the active site gorge of the protein in a fashion similar to that observed with the Alzheimer drug donepezil. The 3D structure of the CPT-11/AChE complex also permits modeling of CPT-11 complexed with mammalian butyrylcholinesterase and carboxylesterase, both of which are known to hydrolyze the drug to the active metabolite. Overall, the results presented here clarify the mechanism of AChE inhibition by CPT-11 and detail the interaction of the drug with the protein. These studies may allow the design of both novel camptothecin analogs that would not inhibit AChE and new AChE inhibitors derived from the camptothecin scaffold.

CPT-11 (Camptosar, irinotecan) is a camptothecin-derived prodrug that is activated by carboxylesterases to yield the potent topoisomerase poison SN-38 (Tanizawa et al., 1994). CPT-11 has demonstrated good antitumor activity against both drug-naive and drug-resistant tumors and is approved for the treatment of colon cancer. It is currently being assessed for efficacy toward a variety of solid tumors in both adults and children (Furman et al., 1999; Saijo, 2003; Simon et al., 2004). As an indication of its remarkable antitumor activity, >90% of children with a variety of solid tumors who had previously undergone multiple cycles of chemotherapy with little or no response demonstrated improvement after CPT-11 administration (Furman et al., 1999). Such efficacy in phase I studies is exceptionally rare.

CPT-11 is a carbamate that requires cleavage by carboxyl-

This work was supported in part by an National Institutes of Health Cancer Center Core grant P30-CA21765 and the American Lebanese Syrian Associated Charities (to P.M.P.), by the U.S. Army Medical Research and Materiel Command (to I.S. and J.L.S.), the Kimmelman Center for Biomolecular Structure and Assembly, the Benoziyo Center for Neurosciences, and the Kalman and Ida Wolens Foundation. The structure was determined in collaboration with the Israel Structural Proteomics Center, supported by the Israel Ministry of Science and Technology, the European Commission Structural Proteomics Project (SPINE) (QLG2-CT-2002-00988), and the Divadol Foundation. J.L.S. is the Morton and Gladys Pickman Professor of Structural Biology.

Article, publication date, and citation information can be found at http://molpharm.aspetjournals.org.

doi:10.1124/mol.104.009944.

ABBREVIATIONS: CPT-11, irinotecan, 7-ethyl-10-[4-(1-piperidino)-1-piperidino]carbonyloxycamptothecin; AChE, acetylcholinesterase; BChE, butyrylcholinesterase; *Ee*AChE, *Electrophorus electricus* acetylcholinesterase; h, human; PB-CPT, 7-ethyl-10-[4-(1-piperazino)-1-benzyl]carbonyl-oxycamptothecin; rCE, rabbit liver carboxylesterase; SN-38, 7-ethyl-10-hydroxycamptothecin; *Tc*AChE, *Torpedo californica* AChE; PDB, protein data bank; RMS, root mean square.

esterases to yield SN-38 (Fig. 1). Both CPT-11 and SN-38 can exist as either a lactone or a hydroxy acid form, with the opening of the E-ring facilitating this process (Pommier et al., 1991). The equilibrium between these two isomers is pH-dependent; thus, at pH 4 both drugs are in the lactone form, at pH 9 they are in the open-ring hydroxyacid form, and at intermediate pH values, both are present (Pommier et al., 1991). The antitumor activity of the hydroxy acid form is much poorer than that of the lactone isomer (Hsiang and Liu, 1988; Pommier et al., 1991). Because the milieu within solid tumors is believed to be acidic in nature, this environment may contribute to the antitumor activity of the drug.

In patients treated with CPT-11, either the levels or the activity of the specific carboxylesterases that activate the drug is low. Hence, in typical single high-dose bolus infusion, <5% of the CPT-11 is converted to SN-38 (Rivory et al., 1997). Consequently, high plasma levels of the parent drug are present for considerable periods of time. CPT-11 is given as the drug rather than SN-38 for several reasons. First, CPT-11 is considerably more water-soluble than SN-38, permitting intravenous infusion. Second, SN-38 is approximately 1000-fold more cytotoxic than CPT-11 and has a very narrow therapeutic "window". This is exemplified by mouse xenograft studies in which at lower doses, no antitumor activity is observed, and at higher doses, severe toxicity is apparent. Indeed, this usually results in significant numbers of animal deaths. CPT-11 does not demonstrate these problems, and therefore, clinical trials have used this drug as the therapeutic agent.

During intravenous administration of CPT-11, typically at doses of 50 to 350 mg/m^2, a cholinergic syndrome is frequently observed (Gandia et al., 1993; Abigerges et al., 1995; Bugat et al., 1995; Petit et al., 1997). This includes rhinitis, increased salivation, miosis, lacrimation, diaphoresis, flushing, and intestinal hyperperistalsis. These symptoms can be rapidly alleviated by atropine, suggesting that the side effects result from interaction of the parent drug with acetylcholinesterase (AChE).

Previous studies have demonstrated that although CPT-11 is an inhibitor of both human (hAChE) and *Electrophorus electricus* AChE (*Ee*AChE) (Kawato et al., 1993; Dodds and Rivory, 1999; Morton et al., 1999), it can be activated by butyrylcholinesterase (BChE). The contribution of the latter enzyme toward antitumor activity is, however, unclear. Recently, Blandizzi and coworkers (2001) reported that AChE was not inhibited by CPT-11 in an in vivo model. To understand the mode of interaction of AChE with CPT-11, we have undertaken a series of biochemical and structural studies with a panel of different AChEs. These included crystallographic experiments using the *Torpedo californica* protein (*Tc*AChE), whose structure has been determined previously (Sussman et al., 1991).

The 3D structure of *Tc*AChE (Sussman et al., 1991) contains a catalytic triad of amino acids (Ser200, His440, and Glu327) lying at the bottom of a deep (approximately 20 Å) gorge. The gorge walls are coated with numerous aromatic side chains. The catalytic binding site, which is responsible for the hydrolysis of acetylcholine, is composed of an acyl binding pocket, an anionic binding site, and an oxyanion hole. The latter orients the acetylcholine ester bond for cleav-

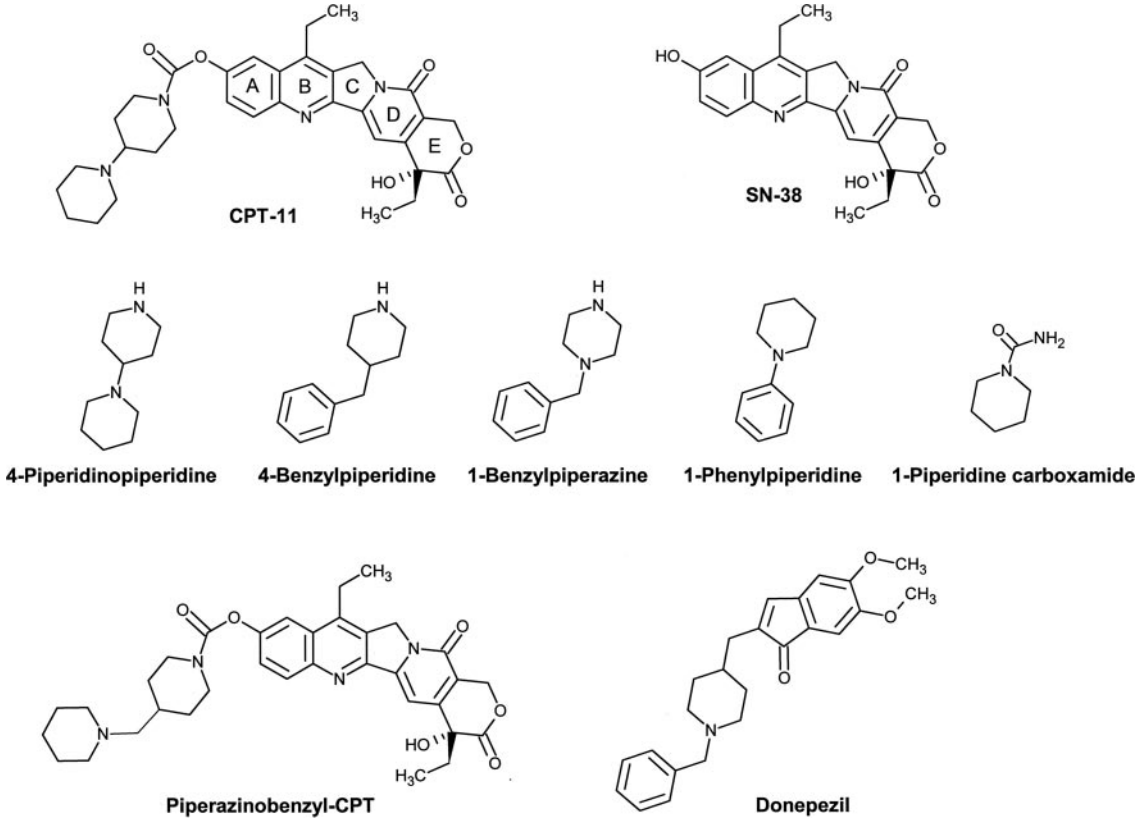

Fig. 1. Chemical structures of CPT-11 and SN-38 (lactone forms) and of 4-piperidinopiperidine, 4-benzylpiperidine, 1-benzylpiperazine, 1-phenylpiperidine, piperidine carboxamide, PB-CPT and donepezil [(±)-2,3-dihydro-5,6-dimethoxy-2-[[1-(phenylmethyl)-4-piperidinyl]methyl]-1*H*-inden-1-one]. The camptothecin rings (A–E) are indicated in CPT-11.

age after it binds to Ser200, and the anionic binding site juxtaposes the positive quaternary ammonium moiety in acetylcholine so that it makes cationic-π interactions with Trp84 (Sussman et al., 1991). At the top of the gorge, there are loops containing a secondary binding site (termed the "peripheral" binding site), which binds bulky inhibitors. This includes compounds that do not penetrate into the gorge and bifunctional inhibitors, which are long enough to span it. The peripheral site contains Trp279, a residue with which both types of inhibitors can make either cationic-π or π–π interactions (Harel et al., 1993). Our structural data show that CPT-11 orients along the active-site gorge of *Tc*AChE analogously to the anti-Alzheimer drug donepezil [(±)-2,3-dihydro-5,6-dimethoxy-2-[[1-(phenylmethyl)-4-piperidinyl]-methyl]-1*H*-inden-1-one], making similar interactions with a series of highly conserved aromatic residues. This orientation precludes attack by the active-site serine on the ester bond, thereby preventing hydrolysis of CPT-11 to yield SN-38.

Materials and Methods

Enzymes, Drugs, and Chemicals. Human AChE (hAChE) and *Ee*AChE were purchased from Sigma-Aldrich (St. Louis, MO). *Tc*AChE was prepared as described previously (Raves et al., 1997; Sussman et al., 1988).

CPT-11 and SN-38 were generous gifts kindly provided by Dr. J. P. McGovren (Pfizer, New York, NY), and donepezil was obtained from the pharmacy of St. Jude Children's Research Hospital (Memphis, TN) as Aricept tablets (Pfizer). PB-CPT (7-ethyl-10-[4-(1-piperazino)-1-benzyl]carbonyloxycamptothecin) was synthesized as described previously (Yoon et al., 2003).

4-Piperidinopiperidine, 4-benzylpiperidine, 1-benzylpiperazine, 1-phenylpiperidine, 1-piperidine carboxamide, acetylthiocholine chloride, and 5,5′-dithiobis-2-nitrobenzoic acid were all obtained from Sigma-Aldrich.

Acetylcholinesterase Inhibition. AChE activity was determined as described previously (Ellman et al., 1961) using 0.5 mM acetylthiocholine as a substrate in 50 mM HEPES, pH 7.4, with modifications as reported by Doctor et al. (1987). Briefly, substrate and inhibitor were pipetted into the individual wells of 96-well plates, and enzyme was then added simultaneously using a multiwell pipettor. Data points were then recorded at 15-s intervals for 2 min. Inhibitor concentrations ranging from 10 pM to 100 μM were assayed, and all data points were measured in duplicate. Data were fitted to the following equation to determine the mode of enzyme inhibition (Webb, 1963):

$$i = \frac{[I]\{[s](1-\beta) + K_s(\alpha-\beta)\}}{[I]\{[s] + \alpha K_s\} + K_i\{\alpha[s] + \alpha K_s\}}$$

where i is fractional inhibition, $[I]$ is inhibitor concentration, $[s]$ is substrate concentration, α is the change in affinity of substrate for enzyme, β is the change in the rate of enzyme-substrate complex breakdown, K_s is the dissociation constant for the enzyme-substrate complex, and K_i is the inhibition constant. An examination of curve fits, with α ranging from 0 to ∞ and β from 0 to 1, was performed using GraphPad Prism software (GraphPad Software Inc., San Diego, CA). The curve generating the highest r^2 value for the curve fit and subsequent statistical analysis were used to assign the mode of enzyme inhibition. K_i values were then calculated from these data sets.

X-Ray Crystallography. *Tc*AChE crystals were grown by the vapor-diffusion method using a 1.5-μl drop of a solution of 10 mg/ml protein mixed with 1.5 μl of mother liquor at 4°C. The mother liquor solution contained 25% polyethylene glycol 600 in 0.05 M HEPES, pH 7.5, and 0.027 M gallamine triethiodide. The latter was added to produce trigonal crystals of space group $P3_221$ (B. Brumshtein, unpublished results). Crystals with dimensions of 0.2 × 0.1 mm grew within 3 weeks. The complex with CPT-11 was obtained by transferring the crystals to a saturated solution of CPT-11 in mother liquor for 16 h. X-ray data were collected from a single crystal on an R-axis diffractometer at 100 K in-house at the Weizmann Institute after washing the mother liquor off the crystal with Parathone N oil. The data were processed using the program XDS (Kabsch, 1993), and the structure was solved by molecular replacement using the $P3_221$-native *Tc*AChE structure as a starting model. Data were refined using Crystallography & NMR System software (Brunger et al., 1998) and fitted using O (Jones et al., 1991). The final CPT-11/*Tc*AChE structure refined to an R-factor of 18.7% and R-free of 23.7%. Data processing and refinement statistics are shown in Table 1.

Overlaying of Protein Structures

CPT-11/*Tc*AChE and Donepezil/*Tc*AChE Crystal Structures. The coordinates of the CPT-11/*Tc*AChE structure were overlaid with the coordinates obtained from the donepezil/*Tc*AChE structure (PDB code 1EVE) (Kryger et al., 1999). The RMS deviation for the two structures was 0.35 Å for 516 Cα atoms.

CPT-11/*Tc*AChE and hBChE Structures. The coordinates of the CPT-11/*Tc*AChE structure were overlaid with the coordinates obtained from the hBChE structure (PDB code 1P0I) (Nicolet et al., 2003). This resulted in a Cα RMS deviation of 0.8 Å for 448 amino acid residues. The CPT-11/hBChE model was then subjected to 90 cycles of energy minimization using the Crystallography & NMR System software (Brunger et al., 1998) to minimize van der Waals clashes between CPT-11 and hBChE. Convergence to a minimum occurred after 90 cycles of refinement and resulted in the total energy decreasing from 6290 to 2819 kcal, and the van der Waals energy decreased from 1575 to 922 kcal.

CPT-11/*Tc*AChE and Rabbit Liver Carboxylesterase Structures. The coordinates of the CPT-11/*Tc*AChE structure were overlaid with the coordinates obtained from the rabbit liver carboxylesterase structure (rCE; PDB code 1K4Y) (Bencharit et al., 2002)). This resulted in a Cα RMS deviation of 0.9 Å for 285 residues. As for the

TABLE 1
Data collection and refinement statistics

Data collection	
Wavelength (Å)	1.54
Unit cell (Å)	137.75, 70.87
Space group	$P3_221$
Resolution range (Å)	30–2.6
Number of unique reflections	23,798
Completeness (%)[a]	98.5 (90.9)
I/σ(I)[a]	10.3 (4.7)
R_{sym}(I) (%)[a]	8.0 (24.0)
Refinement and model statistics	
Resolution range (Å)	30–2.6
Number of reflections	23,820
R-factor[b]: work, free[c] (%)	18.7, 23.7
Average B-factors (Å^2)	39.9
Root mean square deviation from ideal values	
Bond length (Å)	0.007
Bond angle (°)	1.3
Dihedral angles (°)	21.7
Improper torsion angles (°)	0.88
Estimated coordinate error	
Low resolution cutoff (Å)	5.0
ESD from Luzzati plot (Å)	0.28
ESD from SIGMAA (Å)	0.42
Ramachandran outliers (%)	3.3

[a] Data for the outer shell are given in parentheses.
[b] R-factor = $\Sigma||F_o| - |F_c||/\Sigma F_o$, where F_o is the observed amplitude of an X-ray reflection, and F_c is the calculated amplitude of this reflection derived from the refined coordinates.
[c] R-free is the R-factor calculated using 10% of randomly selected reflections. This therefore represents an unbiased measure of the quality of the structural data.

CPT-11/hBChE model, the CPT-11/rCE model was subjected to 90 cycles of energy minimization. The total energy decreased from 4846 to 2256 kcal, and the van der Waals energy decreased from 1536 to 794 kcal.

Results

Inhibition of Various AChEs by CPT-11 and Structurally Related Compounds. To determine the domains within CPT-11 that might be responsible for inhibition of AChE, we performed enzymatic assays using a series of small molecules resembling substructures of the parent drug. Thus, we assessed the ability of 4-piperidinopiperidine, 4-benzylpiperidine, 1-benzylpiperazine, 1-phenylpiperidine, 1-piperidine carboxamide, CPT-11, SN-38, PB-CPT, and donepezil (Fig. 1) to inhibit hAChE, *Ee*AChE, and *Tc*AChE. The data obtained are presented in Table 2. hAChE was effectively inhibited by both CPT-11 and donepezil with K_i values of 51 and 0.88 nM, respectively. SN-38 was a weak inhibitor, with its K_i value being ~400-fold higher than that of CPT-11 and >20,000-fold higher than that of donepezil. This suggested that the camptothecin rings do not significantly contribute to the binding of CPT-11 to AChE. However, 4-piperidinopiperidine, which is the moiety removed from CPT-11 to produce SN-38, was a reasonable inhibitor of hAChE (K_i = 2.92 μM). The structurally related compounds 4-benzylpiperidine, 1-benzylpiperazine, phenylpiperidine, and piperidine carboxamide displayed no inhibition at a maximum concentration of 100 μM. These data indicated that the interaction of the dipiperidino moiety with amino acid residues within AChE was the major factor in enzyme inhibition. This was supported by the results obtained with PB-CPT, which was a ~170- and ~10,000-fold poorer inhibitor of hAChE than CPT-11 and donepezil, respectively.

Comparable results were obtained with *Ee*AChE (Table 2), suggesting that the interaction of the compounds with the two AChEs was similar. Thus, CPT-11 was a very potent inhibitor of *Ee*AChE, with SN-38 demonstrating >100-fold weaker inhibition. As for hAChE, 4-piperidinopiperidine was a much more potent inhibitor of *Ee*AChE than 4-benzylpiperidine, 1-benzylpiperazine, 1-phenylpiperidine, or piperidine carboxamide. Finally, studies with *Tc*AChE confirmed the observations made for the other two AChEs, with both CPT-11 and 4-piperidinopiperidine efficiently inhibiting the enzyme (Table 2).

We wished, therefore, to identify the molecular interactions between CPT-11 and AChE that were responsible for the pattern of inhibition constants displayed in Table 2. Because a substantial number of ligand-protein complexes have been obtained using *Tc*AChE (Sussman et al., 1993; Silman et al., 1994; Harel et al., 1995; Wlodek et al., 1996; Kryger et al., 1999), this enzyme was chosen for the structural studies.

3D Structure of the CPT-11/*Tc*AChE Complex. To determine the 3D structure of the CPT-11/*Tc*AChE complex, a single crystal of *Tc*AChE grown in the presence of gallamine triethiodide (B. Brumstein, M. Harel, J. Sussman, and U. Silman, unpublished data) was soaked in a solution containing CPT-11. The soaked crystal diffracted to 2.6 Å and belonged to the trigonal space group $P3_221$, which was distinct from the $P3_121$ trigonal form originally used to solve the structure of *Tc*AChE (Sussman et al., 1991). In this novel crystal form, the entrance to the active-site gorge is not blocked by a symmetry-related molecule, as is the case for the $P3_121$ form (PDB code 1EA5). However, the RMS deviation of the Cα chain between the $P3_221$ and the $P3_121$ crystal structures was only 0.3 Å, indicating a virtually identical conformation of the two molecules. The electron density allowed tracing of residues 4 to 536 of *Tc*AChE and showed the location of CPT-11 and 241 water molecules. An iodide ion interacting with the side chains of His264 and Glu268 was also observed, which displayed 60% occupancy. For three asparagine residues, Asn59, Asn416, and Asn456, electron density was clearly visible that could be ascribed to the initial residues of attached oligoglycosides. The electron-density map of CPT-11 at 2.6 Å resolution did not permit distinction between the lactone and carboxylate forms at the E-ring. Hence, arbitrarily, the lactone form was refined.

The CPT-11 molecule spanned the active-site gorge (Fig. 2, A and B), interacting with a series of residues from Trp84 at the bottom of the gorge to Phe284 at the top. Nine of the 13 amino acids that interacted with CPT-11 were aromatic (Tyr70, Trp84, Tyr121, Trp279, Phe284, Phe330, Phe331, Tyr334, and His440) (Fig. 3). Because the kinetic data presented above indicated that the piperidinopiperidine moiety made the major contribution toward the binding of CPT-11 to AChE, we also examined the contacts made by the drug in the lower part of the gorge. These primarily included complementary surface contacts with Trp84, Tyr121, Phe331, and His440 and, in particular, a stacking interaction with Phe330. No direct H-bonds were seen between AChE and this portion of CPT-11.

As a consequence of the orientation of CPT-11 within the active-site gorge, the carbamate moiety was positioned adjacent to residues Phe331 and Tyr334. Thus C9, the carbon of the carbamate linkage in CPT-11, was 9.3 Å from Ser200 Oγ, the nucleophilic atom within the catalytic triad. Any attempt to dock CPT-11 closer to Ser200 Oγ (i.e., in a position where hydrolysis could occur) met with failure because of severe

TABLE 2
K_i values for the inhibition of human AChE, *Ee*AChE, and *Tc*AChE by CPT-11 and structurally related compounds

Compound	hAChE			*Ee*AChE			*Tc*AChE		
	K_i ± S.E.	Curve Fit	Mode of Inhibition	K_i ± S.E.	Curve Fit	Mode of Inhibition	K_i ± S.E.	Curve Fit	Mode of Inhibition
	nM	r^2		*nM*	r^2		*nM*	r^2	
CPT-11	50.5 ± 3.9	1.0	P.C.	9.7 ± 2.2	0.94	C	26.4 ± 1.7	1.0	C
SN-38	20,100 ± 3570	0.82	C	1040 ± 250	0.79	C	>100,000	N.A.	N.A.
4-Piperidinopiperidine	2920 ± 520	0.97	P.C.	5300 ± 1840	0.86	C	241 ± 4.2	0.98	C
PB-CPT	8790 ± 1500	0.98	P.C.	N.D.			3990 ± 500	0.94	C
Donepezil	0.88 ± 0.27	0.95	C	0.66 ± 0.13	0.97	C	0.96 ± 0.2	0.98	C

P.C., partially competitive; C, competitive; N.A., not applicable because no inhibition was observed; N.D., not determined.

steric clashes with *Tc*AChE. These data clearly show that *Tc*AChE is not capable of hydrolyzing CPT-11.

Overlay of the CPT-11/*Tc*AChE and Donepezil/*Tc*AChE Crystal Structures. Because the piperidinopiperidine moiety in CPT-11 is structurally homologous to the benzylpiperidino moiety in donepezil, it seemed plausible that the two inhibitors would interact very similarly with amino acids in the active-site gorge. We therefore overlaid the Cα backbones of the CPT-11/*Tc*AChE complex and the donepezil/*Tc*AChE complex (PDB code 1EVE) (Kryger et al., 1999). The resulting overlay of the drug molecules is shown in Fig. 4. The terminal benzene and piperidino domains of donepezil and CPT-11, respectively, and their penultimate heterocyclic rings display substantial overlap. Furthermore, the indanone ring of donepezil and the middle rings of the camptothecin moiety of CPT-11 align almost in the same plane, stacked against the indole ring of Trp279.

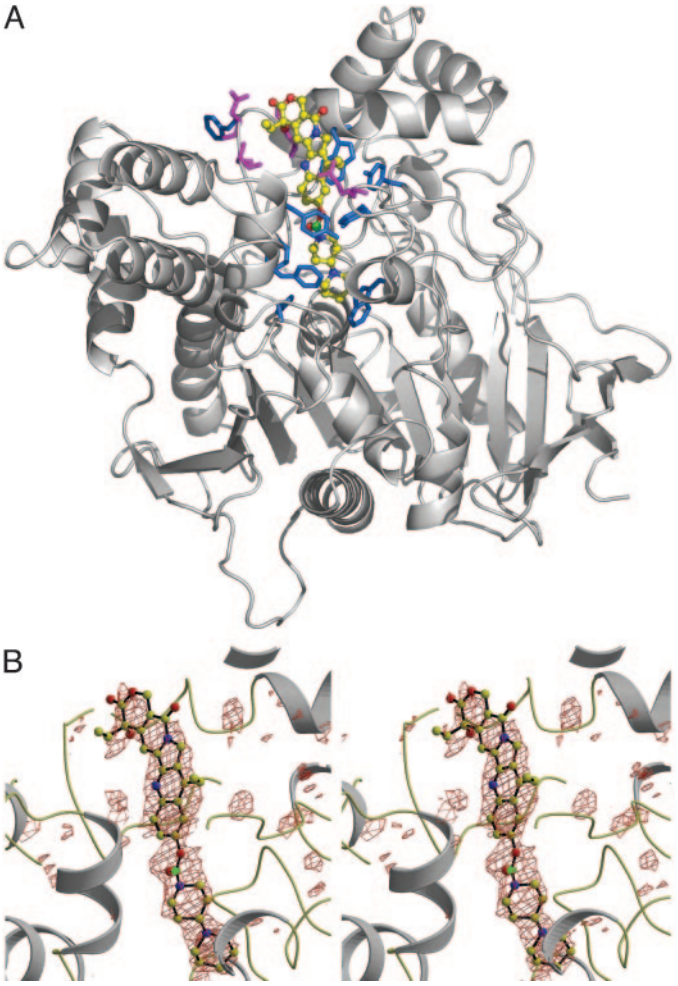

Fig. 2. Crystal structure of *Tc*AChE in complex with CPT-11. A, a view of the active-site gorge with CPT-11 with its carbon atoms color-coded in yellow except for C9 carbon (green), oxygen atoms in red, and nitrogen atoms in blue. Aromatic and nonaromatic amino acid side chains that interact with CPT-11 are shown in blue and magenta, respectively. The figure was made using PyMOL (http://pymol.sourceforge.net). B, a stereo view of the simulated annealing F_o–F_c omit map of CPT-11 at 2.5 σ. CPT-11 atom C9 is shown in green. The figure was drawn using BobScript (Esnouf, 1997) and Raster3D (Merritt and Bacon, 1997). In both figures, the AChE molecule is depicted such that the active-site gorge is vertical with the peripheral site at the top.

Overlay of the CPT-11/*Tc*AChE Complex with the hBChE and the Rabbit Liver Carboxylesterase Structures. Previous studies indicated that although CPT-11 is a potent inhibitor of AChE, both BChE and carboxylesterases can activate the drug to yield SN-38 (Potter et al., 1998; Morton et al., 1999; Khanna et al., 2000). We therefore overlaid the CPT-11/*Tc*AChE structure on that of hBChE (PDB code 1P0I) (Nicolet et al., 2003)). We then modeled the drug within the active-site gorge of hBChE, such that the carbamate carbonyl oxygen was within bonding distance of Ser198 Oγ (i.e., 1.6 Å), the catalytic serine in hBChE. To avoid steric clashes between CPT-11 and the protein, the side chain dihedral angle, χ1, of Trp231 was rotated 110° away from its native conformation. This resulted in a CPT-11/hBChE model with the CPT-11 dipiperidino moiety fitting well in the larger acyl pocket of hBChE.

The X-ray structure of an rCE (PDB code 1K4Y) (Bencharit et al., 2002) was similarly fitted to the CPT-11/*Tc*AChE structure. Here again, CPT-11 was positioned so that the carbamate carbonyl carbon was within bonding distance (i.e., 1.6 Å) of the active-site serine (Ser221). The dipiperidino and camptothecin moieties were subjected to torsion angle rotation to avoid steric clashes with the rCE structure.

Discussion

Several published reports have indicated that the anticancer drug CPT-11 is a potent AChE inhibitor (Kawato et al., 1993; Dodds and Rivory, 1999; Morton et al., 1999). However, recent studies (Blandizzi et al., 2001, 2002) have suggested that this may not be caused by a direct interaction of the drug with the enzyme. To elucidate the interaction of CPT-11 with AChE, we have performed detailed biochemical studies with the drug and with several analogs using three AChEs. Our

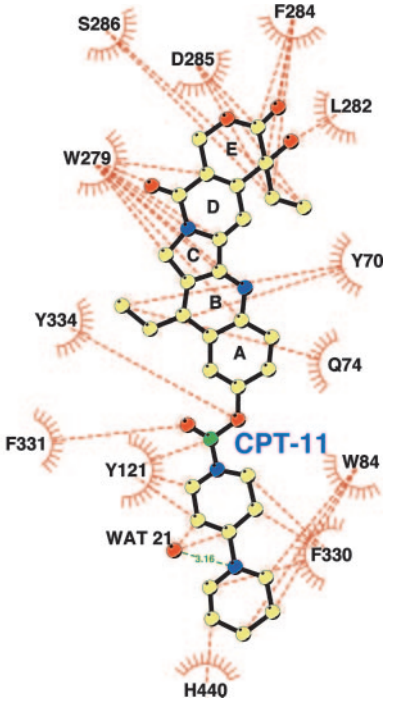

Fig. 3. Interactions of CPT-11 with *Tc*AChE in the CPT-11/*Tc*AChE structure calculated using LIGPLOT (Wallace et al., 1995). Nonbonded interactions are indicated by broken lines. CPT-11 atom C9 is shown in green.

data show that CPT-11 was an effective inhibitor of AChE at concentrations of 9.7 to 51 nM for all three AChEs (Table 2). Furthermore, both the camptothecin rings and the dipiperidino moiety present at the 10 position of the molecule contribute to enzyme inhibition. SN-38, the hydrolysis product of CPT-11, can inhibit AChE at concentrations ranging from 1 to 20 μM; however, because the plasma levels of this drug that can be achieved in patients treated with CPT-11 range from 20 to 150 nM (Rivory et al., 1997), it is unlikely that SN-38 contributes to the inhibition of hAChE in vivo. Conversely, because plasma CPT-11 concentrations as high as 17 μM have been reported in patients after administration of 600 mg/m^2 of the drug (Rivory et al., 1997) and the K_i for the inhibition of hAChE is ~51 nM, it is plausible that the cholinergic syndrome observed in patients with cancer is indeed caused by direct interaction of CPT-11 with AChE. The biochemical studies showed that SN-38 was a poorer inhibitor of *Tc*AChE than hAChE or *Ee*AChE (Table 2). In the latter two proteins, Phe330 is substituted with a tyrosine, and torsional rotation of Tyr330 can bring its hydroxyl group to within hydrogen-bonding distance of the hydroxyl oxygen on the A ring of SN-38. This would probably make SN-38 a better inhibitor of the hAChE and *Ee*AChE than of the *T. californica* enzyme.

All three enzymes were inhibited by both CPT-11 and donepezil (Table 2). Moderate inhibition was also observed with 4-piperidinopiperidine but not with other heterocyclic analogs tested. Thus, the dipiperidino moiety at the 10 position of CPT-11 seems to make a major contribution toward the inhibition of AChE. This was supported by our observation that both SN-38 and PB-CPT poorly inhibited all three AChEs (Table 2). In these two latter compounds, the dipiperidino chemotype is replaced by either a hydroxyl group or by a piperazinobenzyl moiety (Fig. 1). Initial in vitro studies with PB-CPT indicated that it was not a potent antitumor agent (Yoon et al., 2003). This was presumably caused by poor conversion to SN-38 by carboxylesterases. However, we postulated that because CPT-11 contains a piperidino ring, it might interact with AChE in a similar fashion to donepezil. Because the crystal structure of the donepezil/*Tc*AChE complex had been determined previously (Kryger et al., 1999), we decided to determine the structure of the CPT-11/*Tc*AChE complex.

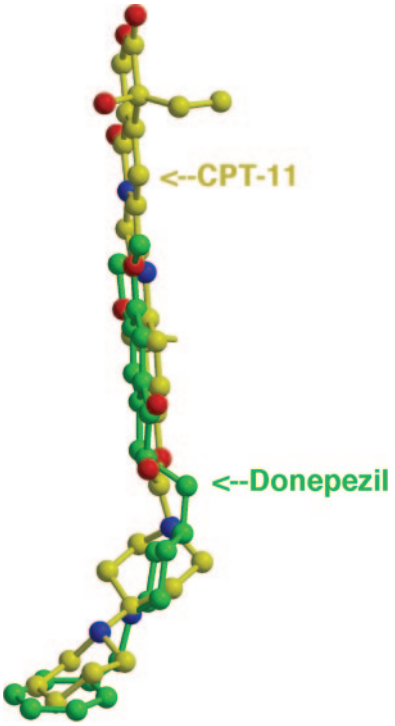

Fig. 4. An overlay of the X-ray structures of CPT-11 and donepezil within their complexes with *Tc*AChE. The overlay of CPT-11 (yellow) and donepezil (green) complexed with *Tc*AChE was achieved by aligning the Cα data for the two structures and then removing the coordinates for both proteins from the image. Hence, the alignment results from almost identical positioning of the drugs within the active-site gorge of *Tc*AChE. The figure was drawn using MolScript (Kraulis, 1991) and Raster3D (Merritt and Bacon, 1997).

The 3D crystal structure of the complex indeed revealed that CPT-11 aligned within the active-site gorge of the enzyme very similarly to donepezil (Fig. 4). Stabilization of the drug in the active site of *Tc*AChE was achieved by eight π–π stacking interactions of the camptothecin rings with aromatic amino acids that line the active-site gorge. In particular, interactions of the fused aromatic rings in CPT-11 with the indole group of Trp279 demonstrated remarkable similarity to the stacking of the indanone moiety of donepezil. Moreover, the penultimate piperidino rings of both CPT-11 and donepezil occupied the same space near the bottom of the gorge, and the aromatic portion of the molecules (i.e., the camptothecin ring and the indanone moiety) both aligned along an identical plane in the *Tc*AChE active site. Thus, the potency of CPT-11 as an AChE inhibitor is a result of several factors. First, the CPT-11 dipiperidino occupies the same space as the piperidino and benzyl rings of donepezil. However, the benzyl group in donepezil stacks against Trp84, whereas in the CPT-11/*Tc*AChE complex, the ultimate piperidino ring which is not aromatic, is tilted by ~30° relative to the benzyl plane. Second, the camptothecin ring system (consisting of four aromatic rings and a cyclic lactone) allows extensive interactions with numerous aromatic residues that line the upper part of the active-site gorge. Finally, the dimensions of CPT-11 and the catalytic gorge are such that a very "snug" fit occurs throughout the entire length of the drug. It is this combination of factors that is responsible for the effective inhibition of AChE by CPT-11.

Although CPT-11 inhibits AChE, it has been demonstrated that BChE can hydrolyze the drug to SN-38 (Dodds and Rivory, 1999; Morton et al., 1999). This implies that the carbamate moiety of CPT-11, located between the dipiperidino moiety and the campthothecin rings, should be within bonding distance of the active-site Ser198 Oγ. The overlay of the CPT-11/*Tc*AChE structure with that of hBChE (PDB code 1P0I) indeed showed that the loop present at the top of the active-site gorge (residues 282–286 in *Tc*AChE) had a different conformation in the two closely related enzymes (Fig. 5). This loop makes numerous interactions with CPT-11 in *Tc*AChE, and the positioning of CPT-11 was such that the interaction of the carbon of the cleaved carbamate bond (C9) with Ser200 Oγ was prevented (Fig. 5a). However, the position of the corresponding loop in hBChE (residues 280–284) does not allow CPT-11 to occupy the upper part of the gorge. Moving the drug down the gorge to avoid clashes with this loop brings the carbamate moiety within bonding distance of Ser198 Oγ. This resulted in a model in which a very snug fit was observed between CPT-11 and the acyl binding pocket of the protein (Fig. 5c). Furthermore, hBChE contains an alanine residue at position 277 (Trp279 in

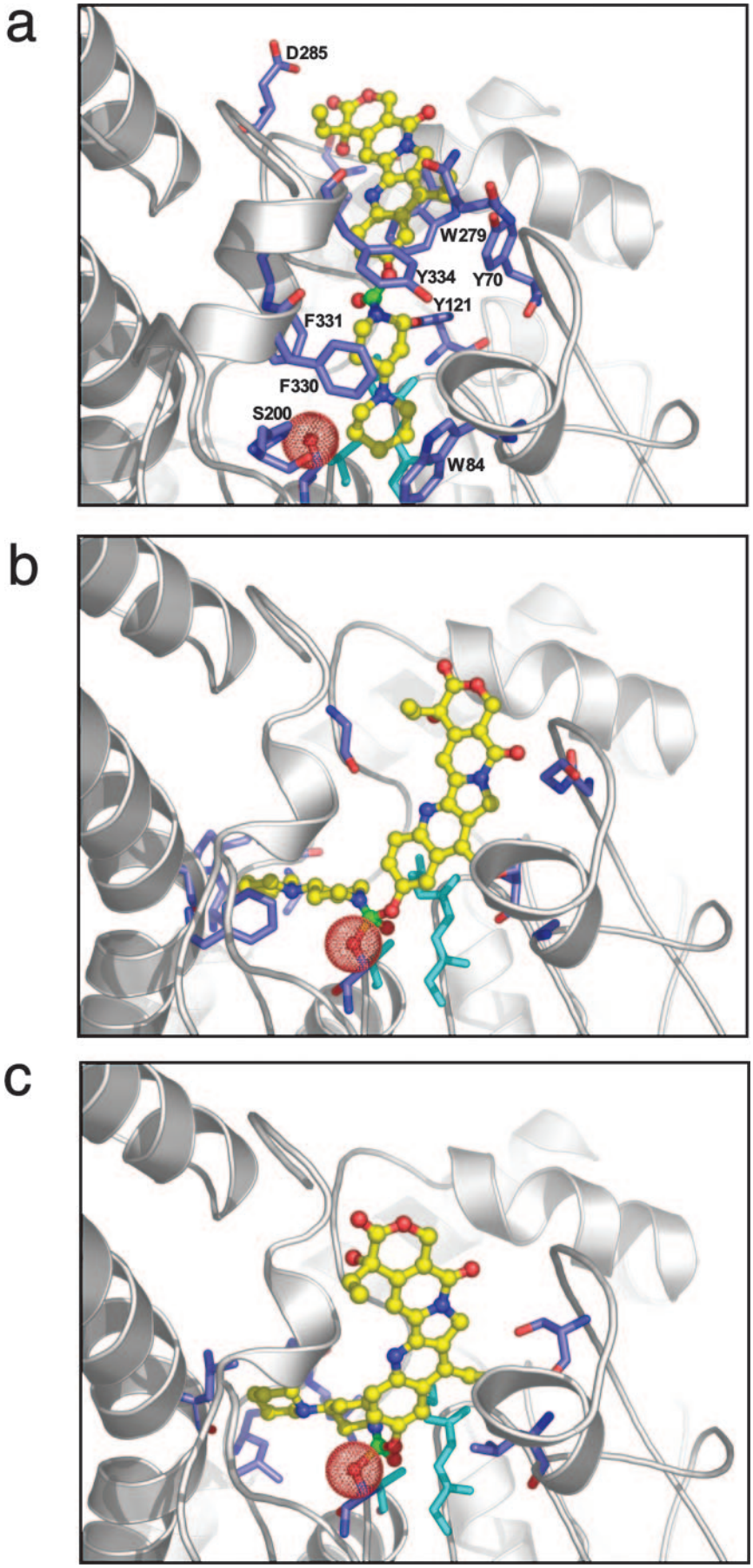

Fig. 5. Comparison of the X-ray structure of the CPT-11/*Tc*AChE complex with the models of CPT-11/hBChE and CPT-11/rCE. a, enlarged view of the active-site gorge in the crystal structure of the CPT-11/*Tc*AChE complex. The polypeptide chain is displayed in a ribbon representation; residues that interact with CPT-11 are shown as blue sticks with oxygen atoms in red. The residues making up the oxyanion hole are shown in cyan, and Ser200 is shown with a red-dotted surface. CPT-11 is color-coded as in Fig. 2a. It is clear that C9 of CPT-11, in green, is too far away to bind covalently to *Tc*AChE Ser200 Oγ, with the two atoms being 9.3 Å apart. b, enlarged view of the active-site gorge in the model of the CPT-11/hBChE complex. The overall alignment and the color-coding is the same as in Fig. 5a. CPT-11 is significantly lower down the active-site gorge, and its position permits the formation of a covalent bond between CPT-11 atom C9 (green) and the active-site Ser198 Oγ (red). c, enlarged view of the active-site gorge in the model of the CPT-11/*r*CE complex. The overall alignment and the color-coding is the same as in Fig. 5a. As in the case of the hBChE model, CPT-11 is significantly further down the active-site gorge than in CPT-11/*Tc*AChE, and its position permits the formation of a covalent bond between CPT-11 atom C9 (green) and the active-site Ser221 Oγ (red). Figures were drawn using PyMOL (http://pymol.sourceforge.net).

*Tc*AChE) that precluded any strong π–π stacking interactions with the camptothecin moiety.

Recently, the X-ray structure of rCE that can efficiently activate CPT-11 has been determined (Bencharit et al., 2002). Although the two enzymes have very different substrate specificities, it is clear that their structures are evolutionarily conserved. However, the structure of rCE in the area corresponding to the peripheral binding site of *Tc*AChE is very different, with Lys301 occupying the position of *Tc*AChE Trp279. In addition, in rCE, as in hBChE, there are no aromatic side chains at the top of the active-site gorge that could make π–π stacking interactions of sufficient strength to prevent CPT-11 from accessing the catalytic triad amino acids. Moreover, the rCE acyl binding pocket has ample space to accommodate the dipiperidino moiety of CPT-11, as is the case for hBChE (Fig. 5c). Hence, the CPT-11/*Tc*AChE structure differs markedly from the models obtained using both the hBChE and rCE X-ray structures. These differences enable us to provide a rational structural explanation for the inhibition of AChE by CPT-11 as opposed to drug hydrolysis by rCE and hBChE.

Overall, the data presented here demonstrate that CPT-11 is a potent inhibitor of AChE and that this is primarily mediated by the piperidino rings binding within the anionic subsite of the protein. In addition, the complex was stabilized by aromatic π–π stacking interactions between the camptothecin moiety and aromatic amino acids that line the active-site gorge, in particular Trp279 within the *Tc*AChE peripheral binding site. These studies have the potential to permit the design of novel AChE inhibitors derived from the camptothecin scaffold and new CPT-11 analogs that would not act as AChE inhibitors and would thus be devoid of the cholinergic side effects.

Acknowledgments

We thank Dr. J. P. McGovren for the gift of CPT-11 and Lilly Toker for preparation of *Tc*AChE.

References

Abigerges D, Chabot GG, Armand JP, Herait P, Gouyette A, and Gandia D (1995) Phase I and pharmacologic studies of the camptothecin analog irinotecan administered every 3 weeks in cancer patients. *J Clin Oncol* **13:**210–221.

Bencharit S, Morton CL, Howard-Williams EL, Danks MK, Potter PM, and Redinbo MR (2002) Structural insights into CPT-11 activation by mammalian carboxylesterases. *Nat Struct Biol* **9:**337–342.

Blandizzi C, Danesi R, De Paolis B, Di Paolo A, Colucci R, Falcone A, and Del Tacca M (2002) Cholinergic toxic syndrome by the anticancer drug irinotecan: acetylcholinesterase does not play a major role. *Clin Pharmacol Ther* **71:**263–271.

Blandizzi C, De Paolis B, Colucci R, Lazzeri G, Baschiera F, and Del Tacca M (2001) Characterization of a novel mechanism accounting for the adverse cholinergic effects of the anticancer drug irinotecan. *Br J Pharmacol* **132:**73–84.

Brunger AT, Adams PD, Clore GM, DeLano WL, Gros P, Grosse Kunstleve RW, Jiang JS, Kuszewski J, Nilges M, Pannu NS, et al. (1998) Crystallography & NMR system: a new software suite for macromolecular structure determination. *Acta Cryst* **54:**905–921.

Bugat R, Rougier P, Douillard JY, Brunet R, Ychou M, Adenis A, Marty M, Seitz JF, Conroy T, Merouche Y, et al. (1995) Efficacy of irinotecan HCl (CPT11) in patients with metastatic colorectal cancer after progression while receiving a 5-FU-based chemotherapy. *Proc Annu Meet Am Soc Clin Oncol* **14:**A567.

Doctor BP, Toker L, Roth E, and Silman I (1987) Microtiter assay for acetylcholinesterase. *Anal Biochem* **166:**399–403.

Dodds HM and Rivory LP (1999) The mechanism for the inhibition of acetylcholinesterases by irinotecan (CPT-11). *Mol Pharmacol* **56:**1346–1353.

Ellman GL, Courtney KD, Anders V, and Featherstone RM (1961) A new and rapid colorimetric determination of acetylcholinesterase activity. *Biochem Pharmacol* **7:**88–95.

Esnouf RM (1997) An extensively modified version of MolScript that includes greatly enhanced coloring capabilities. *J Mol Graph Model* **15:**132–134.

Furman WL, Stewart CF, Poquette CA, Pratt CB, Santana VM, Zamboni WC, Bowman LC, Ma MK, Hoffer FA, Meyer WH, et al. (1999) Direct translation of a protracted irinotecan schedule from a xenograft model to a phase I trial in children. *J Clin Oncol* **17:**1815–1824.

Gandia D, Abigerges D, Armand JP, Chabot G, Da Costa L, De Forni M, Mathieu-Boue A, and Herait P (1993) CPT-11-induced cholinergic effects in cancer patients. *J Clin Oncol* **11:**196–197.

Harel M, Kleywegt GJ, Ravelli RB, Silman I, and Sussman JL (1995) Crystal structure of an acetylcholinesterase-fasciculin complex: interaction of a three-fingered toxin from snake venom with its target. *Structure* **3:**1355–1366.

Harel M, Schalk I, Ehret-Sabatier L, Bouet F, Goeldner M, Hirth C, Axelsen PH, Silman I, and Sussman JL (1993) Quaternary ligand binding to aromatic residues in the active-site gorge of acetylcholinesterase. *Proc Natl Acad Sci USA* **90:**9031–9035.

Hsiang YH and Liu LF (1988) Identification of mammalian DNA topoisomerase I as an intracellular target of the anticancer drug camptothecin. *Cancer Res* **48:**1722–1726.

Jones TA, Zou JY, Cowan SW, and Kjeldgaard (1991) Improved methods for building protein models in electron density maps and the location of errors in these models. *Acta Crystallogr A* **47:**110–119.

Kabsch W (1993) Automatic processing of rotation diffraction data from crystals of initially unknown symmetry and cell constants. *J Appl Cryst* **26:**795–800.

Kawato Y, Sekiguchi M, Akahane K, Tsutomi Y, Hirota Y, Kuga H, Suzuki W, Hakusui H, and Sato K (1993) Inhibitory activity of camptothecin derivatives against acetylcholinesterase in dogs and their binding activity to acetylcholine receptors in rats. *J Pharm Pharmacol* **45:**444–448.

Khanna R, Morton CL, Danks MK, and Potter PM (2000) Proficient metabolism of CPT-11 by a human intestinal carboxylesterase. *Cancer Res* **60:**4725–4728.

Kraulis PJ (1991) MOLSCRIPT: a program to produce both detailed and schematic plots of protein structures. *J Appl Cryst* **24:**946–950.

Kryger G, Silman I, and Sussman JL (1999) Structure of acetylcholinesterase complexed with E2020 (Aricept): implications for the design of new anti-Alzheimer drugs. *Structure* **7:**297–307.

Merritt EA and Bacon DJ (1997) Raster 3D: Photorealistic molecular graphics. *Methods Enzymol* **277:**505–524.

Morton CL, Wadkins RM, Danks MK, and Potter PM (1999) CPT-11 is a potent inhibitor of acetylcholinesterase but is rapidly catalyzed to SN-38 by butyrylcholinesterase. *Cancer Res* **59:**1458–1463.

Nicolet Y, Lockridge O, Masson P, Fontecilla-Camps JC, and Nachon F (2003) Crystal structure of human butyrylcholinesterase and of its complexes with substrate and products. *J Biol Chem* **278:**41141–41147.

Petit RG, Rothenberg ML, Mitchell EP, Compton LD, and Miller LL (1997) Cholinergic symptoms following CPT-11 infusion in a phase II multicenter trial of 250 mg/m2 irinotecan (CRT-11) given every two weeks. Proceedings of the 33th Annual Meeting of the American Society for Clinical Oncology; 1997 May 17–20; Denver, Colorado. **16:**A953.

Pommier Y, Jaxel C, Kerigan D, and Kohn KW (1991) Structure activity relationship of topoisomerase I inhibition by camptothecin derivatives: evidence for the existence of a ternary complex, in *DNA Topoisomerases in Cancer* (Potmesil M and Kohn KW eds) pp 121–132, Oxford University Press, New York.

Potter PM, Pawlik CA, Morton CL, Naeve CW, and Danks MK (1998) Isolation and partial characterization of a cDNA encoding a rabbit liver carboxylesterase that activates the prodrug irinotecan (CPT-11). *Cancer Res* **52:**2646–2651.

Raves ML, Harel M, Pang YP, Silman I, Kozikowski AP, and Sussman JL (1997) Structure of acetylcholinesterase complexed with the nootropic alkaloid, (−)-huperzine A. *Nat Struct Biol* **4:**57–63.

Rivory LP, Haaz M-C, Canal P, Lokiec F, Armand J-P, and Robert J (1997) Pharmacokinetic interrelationships of irinotecan (CPT-11) and its three major plasma metabolites in patients enrolled in Phase I/II trials. *Clin Cancer Res* **3:**1261–1266.

Saijo N (2003) Progress in treatment of small-cell lung cancer: role of CPT-11. *Br J Cancer* **89:**2178–2183.

Silman I, Harel M, Axelsen P, Raves M, and Sussman JL (1994) Three-dimensional structures of acetylcholinesterase and of its complexes with anticholinesterase agents. *Biochem Soc Trans* **22:**745–749.

Simon M, Argiris A, and Murren JR (2004) Progress in the therapy of small cell lung cancer. *Crit Rev Oncol Hematol* **49:**119–133.

Sussman JL, Harel M, Frolow F, Oefner C, Goldman A, Toker L, and Silman I (1991) Atomic structure of acetylcholinesterase from *Torpedo californica*: a prototypic acetylcholine-binding protein. *Science (Wash DC)* **253:**872–879.

Sussman JL, Harel M, Frolow F, Varon L, Toker L, Futerman AH, and Silman I (1988) Purification and crystallization of a dimeric form of acetylcholinesterase from *Torpedo californica* subsequent to solubilization with phosphatidylinositol-specific phospholipase C. *J Mol Biol* **203:**821–823.

Sussman JL, Harel M, and Silman I (1993) Three-dimensional structure of acetylcholinesterase and of its complexes with anticholinesterase drugs. *Chem Biol Interact* **87:**187–197.

Tanizawa A, Fujimori A, Fujimori Y, and Pommier Y (1994) Comparison of topoisomerase I inhibition, DNA damage and cytotoxicity of camptothecin derivatives presently in clinical trials. *J Natl Cancer Inst* **86:**836–842.

Wallace AC, Laskowski RA, and Thornton JM (1995) LIGPLOT: a program to generate schematic diagrams of protein-ligand interactions. *Prot Engineer* **8:**127–134.

Webb JL (1963) *Enzyme and Metabolic Inhibitors. Volume 1. General Principles of Inhibition*, p 57, Academic Press, New York.

Wlodek ST, Antosiewicz J, McCammon JA, Straatsma TP, Gilson MK, Briggs JM, Humblet C, and Sussman JL (1996) Binding of tacrine and 6-chlorotacrine by acetylcholinesterase. *Biopolymers* **38:**109–117.

Yoon KJ, Krull EJ, Morton CL, Bornmann WG, Lee RE, Potter PM, and Danks MK (2003) Activation of a camptothecin prodrug by specific carboxylesterases as predicted by quantitative structure-activity relationship and molecular docking studies. *Mol Cancer Ther* **2:**1171–1181.

Address correspondence to: Dr. Philip M. Potter, Department of Molecular Pharmacology, St. Jude Children's Research Hospital, 332 N. Lauderdale, Memphis, TN 38105. E-mail: phil.potter@stjude.org